A Reflectivity Climatology Algorithm for Hybrid Scans and Its Application to Radar Coverage over the Tibetan Plateau

ZHUANG Wei[1,2*] (庄 薇) and LIU Liping[1] (刘黎平)

1 *State Key Laboratory of Severe Weather, Chinese Academy of Meteorological Sciences, Beijing* 100081

2 *Nanjing University of Information Science and Technology, Nanjing* 210044

(Received December 9, 2011; in final form September 7, 2012)

ABSTRACT

The traditional algorithm for hybrid radar scans uses standard terrain digital elevation model (DEM) data and the latitudes, longitudes and altitudes of contributing radar stations. While radar station location information is often inaccurate, signal blockages due to trees, buildings, and other surface objects are not included in the DEM data. Accordingly, hybrid scan elevations derived using this traditional algorithm are prone to errors. Here, reflectivity climatology data (the frequency of occurrence of reflectivity) are used to improve the algorithm for hybrid scans. Three parameters are introduced, then applied to evaluation of signal blockage for every radar bin using a fuzzy logic technique. This new algorithm provides an improved determination of the lowest unblocked elevation for hybrid scans. The new algorithm is validated by examining the scope and continuity of the calculated hybrid scan reflectivity in a case study, and the performance of this climatology-based algorithm is evaluated relative to the traditional terrain-based algorithm. The climatology-based hybrid scans are then used to examine the spatial coverage provided by the operational weather radar network over the Tibetan Plateau. The results indicate that the terrain-based hybrid scan algorithm introduced errors that caused obvious V-shaped gaps in hybrid scan reflectivity. By contrast, the climatology-based hybrid scan algorithm more accurately determined the lowest unblocked elevation and reduced the impacts of blockage. The coverage map illustrates the limitations of the weather radar network over the Tibetan Plateau. These limitations inhibit the usefulness of the radar data. Additional radar or observational data are needed to fill these gaps and minimize the impacts of signal blockage.

Key words: hybrid scans, reflectivity climatology, complex terrain, radar coverage, Tibetan Plateau

Citation: Zhuang Wei and Liu Liping, 2012: A reflectivity climatology algorithm for hybrid scans and its application to radar coverage over the Tibetan Plateau. *Acta Meteor. Sinica*, **26**(6), 746–757, doi: 10.1007/s13351-012-0606-1.

1. Introduction

Radar beam blockage reduces the quality of radar data and restricts its applications over complex terrains (Pellarin et al., 2002); accordingly, beam blockage is one of the problems that must be considered in determining the optimal locations of weather radar sites (Bandalo, 1992). Complex terrain introduces inevitable blockages around the radar site, affecting the quality of radar data at lower elevations. The radar reflectivity at these lower elevations is the most useful information for estimating surface precipitation, especially in areas of complex terrain (Joss and Waldvogel, 1990; Sauvageot, 1994). Hybrid radar scans include only the lowest radar bins that do not have significant blockages (O'Bannon, 1997). These radar bins, which may result from different tilts at different locations, consist of two-dimensional polar coordinate grids. Hybrid scans play an important role in reducing the impacts of radar beam blockages and improving radar estimates of precipitation (Chang et al., 2009). These scans are also highly useful for analyzing the spatial coverage of weather radar networks (Maddox et al., 2002).

The NOAA National Severe Storms Laboratory (NSSL) developed an automatic hybrid scan algorithm

Supported by the Chinese Academy of Meteorological Sciences Basic Scientific and Operational Project, National Basic Research and Development (973) Program of China (2012CB417202), and China Meteorological Administration Special Public Welfare Research Fund (GYHY201006042).

*Corresponding author: zhuangwei@cams.cma.gov.cn.

(O'Bannon, 1997). It is based on the terrain, radar beam model (or power density function), and propagation path of a radar beam. This algorithm calculates the beam blockage rate and hybrid scan angle of elevation, and depends on terrain data rather than the radar mode and scan strategy. Hybrid scans using this algorithm have been widely used in WSR-88D operational radar networks over standard terrains (Fulton et al., 1998), and have improved quantitative estimates of precipitation in regions of complex terrain (Morin and Gabella, 2007).

Chinese scientists have evaluated hybrid scans by calculating beam blockage rate (Yang et al., 2009; Xiao et al., 2008a, b); however, the beam blockage information in these algorithms is determined under the assumption of standard beam propagation and only accounts for major blockages. The actual blockages and clutter distributions can deviate from these assumptions due to anomalous beam propagation, clutter contamination from side lobes, and blockage by trees and buildings that are not included in terrain data.

Reflectivity climatologies have been used to study the distributions of precipitation in a variety of geographical regions (Kuo and Orville, 1973; Steenburgh et al., 2000; Heinselman and Schultz, 2006). This method has also been used to build rainfall detection maps that account for beam blockages not represented under standard propagations (e.g., Krajewski and Vignal, 2001). These studies suggest that reflectivity climatologies can provide useful information in areas of complex terrain, where quantitative precipitation estimates based on radar observations are often problematic due to signal blockage.

The Tibetan Plateau, which is over 4500 m above sea level, greatly affects the weather and climate of southeastern China, eastern Asia, and even the world (Xu and Chen, 2006). The objective of the third Tibetan Plateau atmospheric science experiment is to clarify the mechanisms that control the energy and water cycles of the Tibetan Plateau and surrounding areas, as well as the effects of these cycles on regional and global climate. This experiment requires a variety of data, including a reanalysis platform, satellite remote sensing observations, and comprehensive surface observations. Weather radar observations are an important component of the surface observational network, and are useful for understanding the role of cloud and precipitation processes in the water cycle over the Tibetan Plateau (Liu et al., 2002). However, the application of radar observations over the Tibetan Plateau is limited by severe beam blockage associated with the complex terrain. To present, little research has been done to examine this problem. Hybrid scans can minimize the impact of terrain on radar observation data; however, the hybrid scan elevations calculated using the traditional terrain-based algorithm are often inaccurate because standard terrain data do not account for trees, buildings, and other surface objects (Chang et al., 2009). Therefore, one important step toward developing a more useful radar network is to construct a hybrid scan algorithm that does not rely on terrain data and radar location. Such an algorithm would reduce the impact of terrain on radar data, enhancing the utility of the new-generation weather radar network to studies of cloud and precipitation processes over the Tibetan Plateau.

In this study, three months of radar data from May to July 2010 are analyzed to investigate the characteristics of the beam blockage distributions for radars over the Tibetan Plateau. A new hybrid scan algorithm based on the reflectivity climatology is developed. Section 2 describes the data used to derive the reflectivity climatology. Section 3 describes the methodology used to identify blockages in the reflectivity climatology and the derivation of the hybrid scan algorithm based on this climatology. Section 4 presents a comparison of hybrid scans made using the new reflectivity climatology-based algorithm to scans made using the traditional terrain-based algorithm. Section 5 provides an analysis of the radar coverage over the Tibetan Plateau. The results are summarized in Section 6.

2. Data

2.1 Radar and terrain data

The radar data used in this paper are from two operational Doppler radars in the Qinghai weather radar network. One of the radars is located in Xining while

Table 1. Parameters of the radar stations

	Mode	Longitude	Latitude	Elevation (m)	Gate number
Xining	CD	101.7750°E	36.5978°N	2446	1000
Haibei	CD	100.9100°E	36.9500°N	3132	1000

the other is located in Haibei. Both radars operate on a 5.5-cm wavelength (C band) with a beam width of 1°. Both radars also share the same scan mode, with a volume coverage pattern (VCP) of 21 with 9 elevation angles (0.5°, 1.5°, 2.4°, 3.4°, 4.3°, 6.0°, 9.9°, 14.6°, and 19.5°). A single scan takes 5–6 min to complete. Table 1 lists the radar parameters, including mode, longitude, latitude, elevation, and gate number.

The terrain data are 1/250-K digital elevation model (DEM) data with a resolution of 0.0008333°×0.0008333°, and are provided by the State Bureau of Surveying and Mapping of China.

2.2 Frequency of occurrence of reflectivity

The radar reflectivity climatology is defined as the frequency of occurrence of reflectivity (FOR) that exceeds a certain threshold. The climatology is calculated on a pixel-by-pixel basis in (spherical) coordinates (similar to Krajewski and Vignal, 2001).

$$\mathrm{FOR}(j,i,k) = \frac{n}{N} \times 100\%, \tag{1}$$

where N is the number of total volume scans, n is the number of scans with reflectivity higher than the threshold, and i, j, and k indicate the ordinal numbers of the radar bins in the azimuthal, range, and elevation directions, respectively. The values of FOR range from 0 to 1, with 0 indicating that no radar echoes higher than the threshold are detected (e.g., the location is obscured by an object that completely blocks the radar beam) and 1 indicating that echoes are detected for all scans (e.g., power return from a stationary object, such as a tall building or mountain). Approximately 21600 volume scans have been obtained from the Xining radar over the three continuous months from May to July 2010. These volume scans are used to analyze the relationship between FOR and beam blockage. Figures $1a_1$–$1f_1$ show maps of FOR (> –32 dBZ) for the first through sixth tilts of the Xining radar, while Figs. $1a_2$–$1f_2$ show the radar reflectivity of a precipitation event at 0340 UTC 16 July 2010 observed by the first through sixth tilts of the Xining radar.

The frequency of occurrence of reflectivity and the hybrid scan reflectivity (Fig. 1) are strongly correlated, with the lowest five tilts of the Xining radar blocked to varying degrees. The radar reflectivity is missing and the value of FOR is 0 when the radar beam is completely blocked. The value of reflectivity is lower in partially blocked radial sectors than in adjacent unblocked radial sectors. The reflectivity is continuous when the radar beam is unblocked, and the value of FOR exceeds that of blocked areas at the same radial distance. The purposes of this paper are (1) to identify sectors that have no blockages and (2) to determine the lowest unblocked tilt angle of the radar for sectors with blockages (i.e., the hybrid scan elevation).

3. Construction of hybrid scans by reflectivity climatology

3.1 Blockage discrimination method

3.1.1 Discrimination parameters

To calculate hybrid scans, it is first necessary to identify blockage. This paper suggests the use of three parameters to identify blockages. These parameters can be deduced by analyzing the sample distribution functions derived from the calibration dataset (where all FOR values have been manually labeled as blocked, partially blocked or unblocked). The three relevant parameters comprise the relative frequency of occurrence of reflectivity (RFOR), the azimuthal variety of frequency of occurrence of reflectivity (AVFOR), and the vertical variety of frequency of occurrence of reflectivity (VVFOR). Calculation of these three parameters is conducted in a polar coordinate system, with determination of each azimuthal direction and the slant-range of every elevation angle. The resolution is 1°×0.25 km (radial resolution × gate width) with a horizontal range of 250 km. The parameters are determined as follows.

1) Relative frequency occurrence of reflectivity

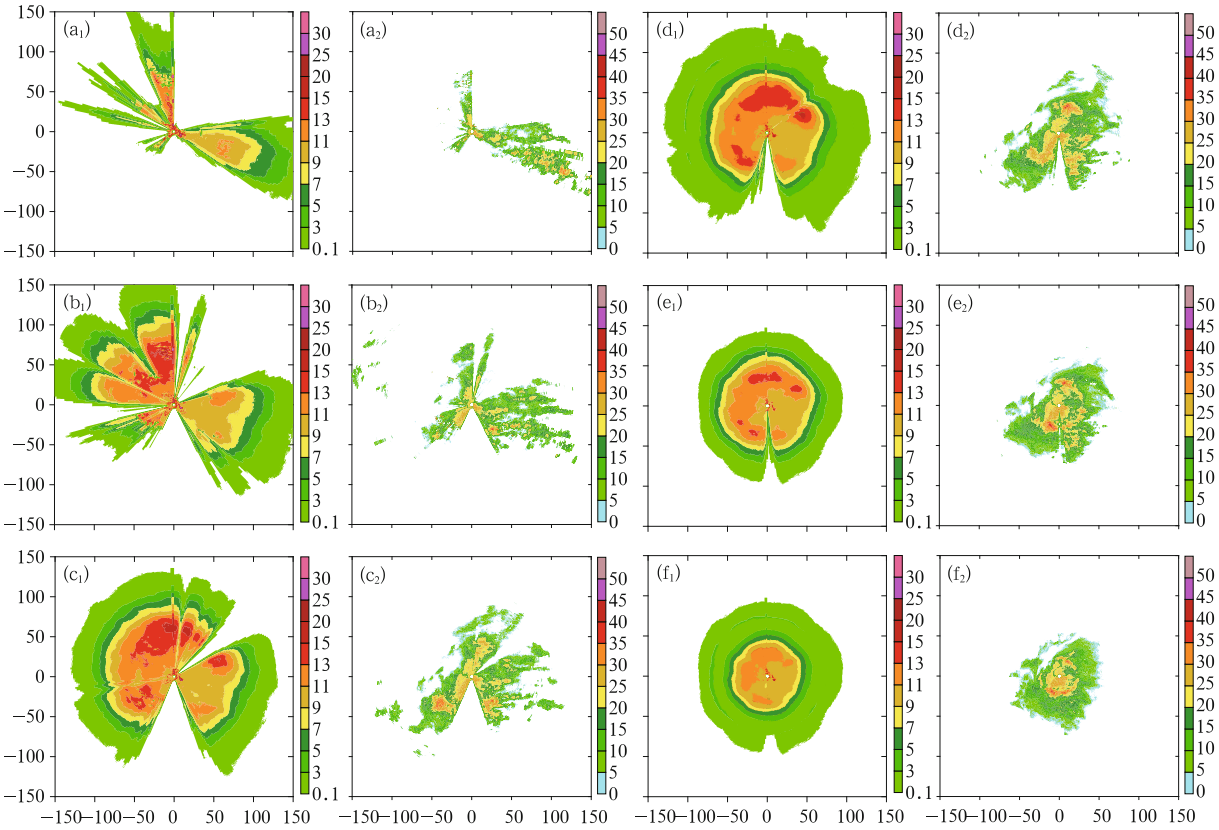

Fig. 1. (a_1–f_1) FOR of reflectivity > –32 dBZ from the first tilt (a_1) to the sixth tilt (f_1) of the Xining radar; (a_2–f_2) radar reflectivity observed by the Xining radar at 0340 UTC 16 July 2010 from the first tilt (a_2) to the sixth tilt (f_2).

(RFOR)

$$\mathrm{RFOR}(j,i,k)=\left(\frac{\mathrm{FOR}(j,i,k)}{\mathrm{MFOR}(j,k)}\right)^2, \tag{2}$$

$$\mathrm{MFOR}(j,k)=\sum_{i=1}^{N_\mathrm{a}}\frac{\mathrm{FOR}(j,i,k)}{n}. \tag{3}$$

FOR is the frequency of occurrence of reflectivity (see Eq. (1)). FOR is more representative when more radar volume scans are used. MFOR is the mean value of FOR at the same range distance from the radar (Eq. (3)). The indices i, j, and k indicate the ordinal numbers of the radar bins in the azimuthal, range, and elevation directions, respectively, and N_a stands for the total number of azimuthal bins.

The relative frequency of occurrence of reflectivity (RFOR) accounts for the fact that if some azimuths are partly blocked and other azimuths are unblocked, FOR will generally be higher in the unblocked areas than MFOR at the same range from the radar site. By contrast, FOR in partially blocked areas will generally be lower than MFOR at the same range from the radar site.

2) Azimuthal variation of frequency of occurrence of reflectivity (AVFOR)

$$\mathrm{AVFOR}(j,i,k)=\sqrt{|[\mathrm{FOR}(j,i+2,k)-\mathrm{FOR}(j,i-1,k)]\times[\mathrm{FOR}(j,i+1,k)-\mathrm{FOR}(j,i-2,k)]|}. \tag{4}$$

AVFOR accounts for the fact that the boundary regions between completely blocked and unblocked regions have evident gradients in FOR along the tangential direction. The tangential gradient in FOR is typically smaller in uniformly unblocked regions.

3) Vertical variation of frequency of occurrence of reflectivity (VVFOR)

$$\mathrm{VVFOR}(j,i,k)=\frac{\mathrm{FOR}(j,i,k+1)-\mathrm{FOR}(j,i,k)}{\mathrm{HEIGHT}(j,i,k+1)-\mathrm{HEIGHT}(j,i,k)}, \tag{5}$$

where HEIGHT indicates the vertical distance betw-

een the radar bin and the ground. The height difference between beams at two elevation angles increases with distance from the radar. VVFOR accounts for the fact that, in unblocked regions, FOR is typically larger at lower elevations than at higher elevations. In partially blocked areas, the opposite is typically true: FOR is generally less at lower elevations than at higher elevations.

3.1.2 Statistical features of blockage identification parameters

The ideal statistical characteristics should be derived from numerous samples that cover actual unblocked and partially blocked areas, including samples that encompass a variety of ranges and elevation angles. Partially blocked and unblocked areas at each elevation are discriminated by artificial determination through analysis of the FOR and reflectivity for a large-scale precipitation case (Fig. 1). The three discrimination parameters RFOR, AVFOR, and VVFOR are calculated from the FOR values for the unblocked and partially blocked areas. Figure 2 shows the distribution frequencies of RFOR, AVFOR, and VVFOR. The partially blocked areas have lower values of RFOR but higher values of AVFOR and VVFOR. Furthermore, the spatial variability tends to be greater in partially blocked sections than in unblocked sections.

3.1.3 Fuzzy logic technique for identifying blockage

The distribution frequency density curves of the parameters for discrimination between the unblocked and partially blocked sections intersect; accordingly, unblocked and partially blocked areas cannot be completely discriminated using fixed parameter thresholds. We therefore suggest using a fuzzy logic method (FLM) to distinguish the unblocked areas from the partially blocked areas. The most relevant characteristic of FLM is that it does not require detailed quantitative values of discrimination parameters; rather, it divides the parameters into various categories and then applies loose classification rules to determine an optimal result. This approach is characterized by good extensibility and compatibility. The traditional FLM (Mendel, 1995; Zadeh, 1965) covers four stages: fuzziness, rule judgment, integration, and de-aliasing. In this paper, concrete system structures are constructed by taking the three discrimination parameters RFOR, AVFOR, and VVFOR as input parameters. The output parameters then indicate whether a region is partially blocked or unblocked. Triangular membership functions with a basic trigonometric form are used to deal with the fuzziness of the three discrimination parameters. The formula is given by

$$Y = \begin{cases} 0, & X \leqslant x1,\ X \geqslant x3; \\ 100 \times \dfrac{X - x1}{x2 - x1}, & x1 < X \leqslant x2; \\ 100 \times \dfrac{x3 - X}{x3 - x2}, & x2 < X \leqslant x3. \end{cases} \tag{6}$$

The distribution frequency density of each parameter in Fig. 2 is used to determine the membership function thresholds for unblocked and partially blocked areas. Fuzziness is accounted for by using the membership function to turn the input parameters into a fuzzy base. Figure 3 presents the fuzzy

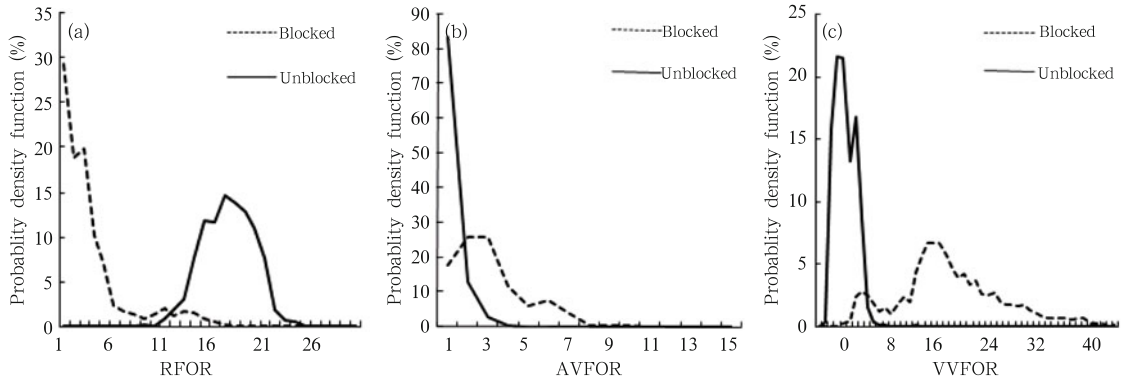

Fig. 2. Probability densities of (a) RFOR, (b) AVFOR, and (c) VVFOR in unblocked (solid) and partially blocked (dashed) regions.

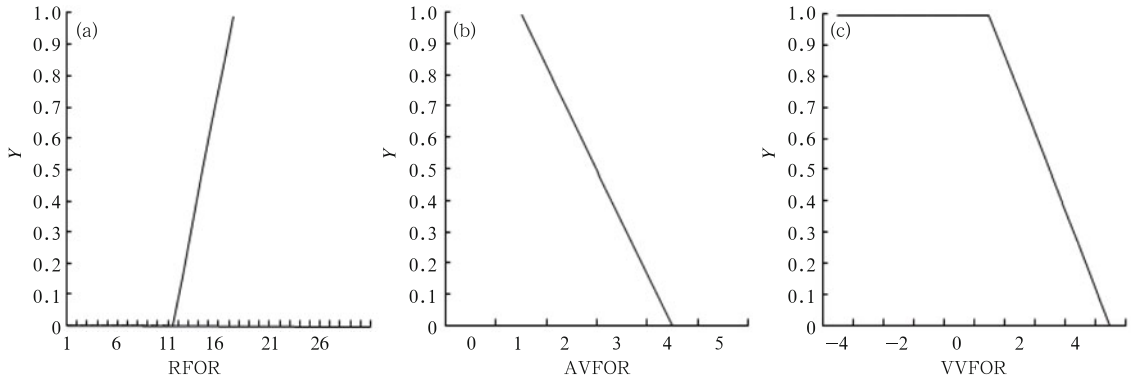

Fig. 3. Membership functions for (a) RFOR, (b) AVFOR, and (c) VVFOR.

base for unblocked areas that accords with the membership functions for the three discrimination parameters discussed above. Rule deduction is equivalent to the calculation of the conditional probability functions for the unblocked and partially blocked regions:

$$P = \sum_{l=1}^{n} w_l P_l, \tag{7}$$

where l indexes the input parameters, n is the number of parameters ($n = 3$ in this case), P_l indicates the contribution of parameter l to the probability that an area is unblocked (the value of P_l is equal to Y_l), and w_l indicates the weight of parameter l, with $\sum_{l=1}^{n} w_l = 1$. P is the conditional probability that an area is unblocked. If $P \geqslant 0.5$, the area is classified as unblocked, while if $P < 0.5$, it is classified as partially blocked. This classification is applied to the full three-dimensional distribution of conditional probabilities $P(j, i, k)$ (evaluated for each combination of radar range bin j, azimuthal direction bin i, and elevation bin k) to determine the lowest unblocked elevation angle at each horizontal location, $\mathrm{Ele}_{\min}(j, i)$. This information can then be used to construct hybrid scans.

3.2 Construction of hybrid scans algorithm

The unblocked conditional distribution $P(j, i, k)$ allows us to evaluate whether the radar beam is partially blocked or not at elevation k, azimuth i, and range j. Proceeding from low elevations to high elevations, identification of the first $P(j, i, k) \geqslant$ threshold in a radar bin establishes the lowest elevation angle for which the radar beam is unblocked. By contrast, identification of $P(j, i, k) <$ threshold indicates an elevation angle that is partially blocked; the condition $P(j, i, k + 1)$ of the next lowest elevation angle must then be examined. This procedure is iterated until the lowest unblocked elevation angle $\mathrm{Ele}_{\min}(j, i)$ is identified for all radar bins (j, i). Hybrid scans can then be constructed using this information.

Figure 4a shows the hybrid scan elevations the Xining determined from reflectivity climatology using blockage discrimination and radar FOR from continuous volume radar scans at Xining between May and July 2010. This figure shows that the radar in is severely affected by blockage. The radar coverage of all but the eastern and northwestern areas requires elevation angles greater than 2.4°. The blockage is most severe in the southern azimuthal direction, with radar coverage blocked at elevation angles below 6.0°.

The hybrid scan reflectivity (HSR) is defined as the reflectivity factor that corresponds to the hybrid scan elevation for each radar bin. Figure 4b shows the HSR derived using volume scan data from the Xining radar at 0340 UTC 16 July 2010. Comparison to the radar reflectivity evaluated at each elevation angle between the first and sixth tilts (Figs. $1a_2$–$1f_2$) indicates that the HSR is unaffected by discontinuities while retaining the spatial scope of the original data. This improvement indicates that the hybrid scan method introduced above can effectively discriminate between the partially blocked and unblocked sections of the Xining weather radar, that the identified hybrid

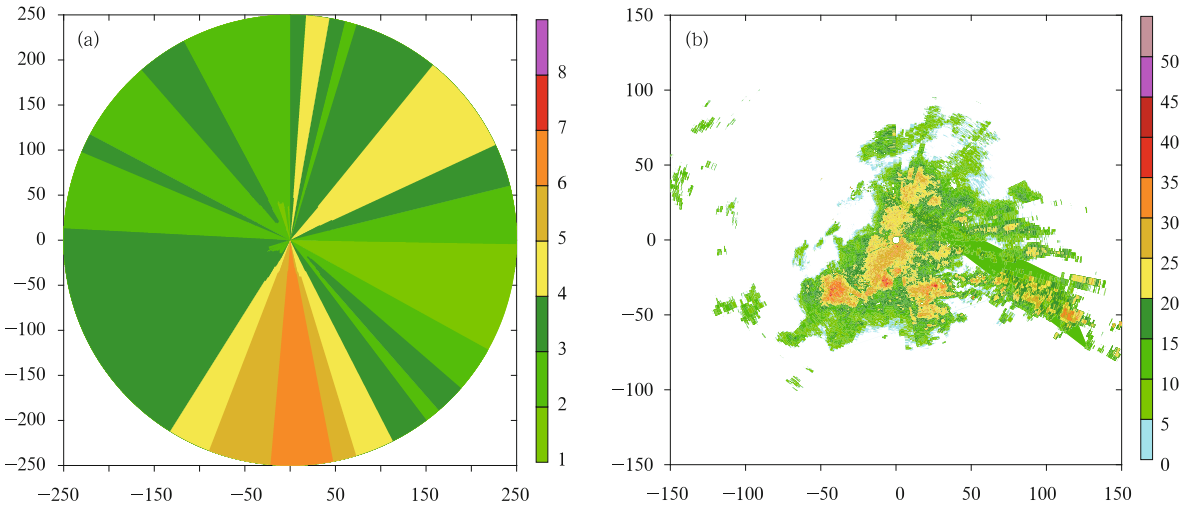

Fig. 4. (a) The hybrid scan elevation (m) for the Xining radar and (b) the hybrid scan reflectivity (dBZ) observed by the Xining radar at 0340 UTC 16 July 2010.

scan elevations are reliable, and that the hybrid scan reflectivity can be used for quantitative precipitation estimation (QPE).

4. Evaluation of the hybrid scan method

4.1 Comparison and analysis of two methods of hybrid scans

The traditional algorithm for obtaining hybrid scans uses standard terrain DEM data along with the latitude, longitude and altitude of radar stations to calculate the radar beam blockage rate. The rationality of this hybrid scans algorithm is reflected in the resulting HSR, which is continuous and effective over a large spatial range. In this section, the HSR generated by the traditional terrain-based hybrid scan algorithm is compared with that generated by the reflectivity climatology-based algorithm described above. This comparison is performed in the context of a large-scale stratiform precipitation event.

Figure 5 shows the hybrid scan elevations for the terrain-based and reflectivity climatology-based hybrid scans along with the corresponding HSR. Terrain-based hybrid scans for the Xining radar are completely free from blockage at the fifth tilt (Fig. $5a_1$), whereas the reflectivity climatology-based hybrid scans are not free from blockage until the sixth tilt (Fig. $5a_2$).

Comparison of the HSR obtained from the Xining radar by hybrid scans based on the two different algorithms (Figs. $5b_1$ and $5b_2$) indicates that the terrain-based algorithm potentially creates three V-shaped gaps in HSR. For the first gap (solid arrow), the reflectivity climatology-based algorithm indicates that the hybrid scan elevation is the third tilt, while the terrain-based algorithm determines that the hybrid scan elevation is the second tilt. For the second gap (dashed arrow), the reflectivity climatology-based algorithm indicates that the hybrid scan elevation is the fourth tilt, while the terrain-based algorithm identifies the third tilt. For the third gap (dashed circle), the reflectivity climatology-based algorithm identifies the sixth tilt, while the terrain-based algorithm identifies the fifth tilt. These three V-shaped gaps are created because the terrain-based hybrid scan elevations in these locations are lower than the actual lowest unblocked elevation angle. These gaps do not appear in the HSR calculated using the reflectivity climatology-based algorithm.

Gaps in HSR can also be created by the identification of hybrid scan elevations that are higher than the lowest unblocked tilt, because radar coverage at higher tilts is not so extensive as radar coverage at lower tilts.

The advantage of the reflectivity climatology method is that it can accurately calculate the lowest unblocked elevation for use in hybrid scans. The iden-

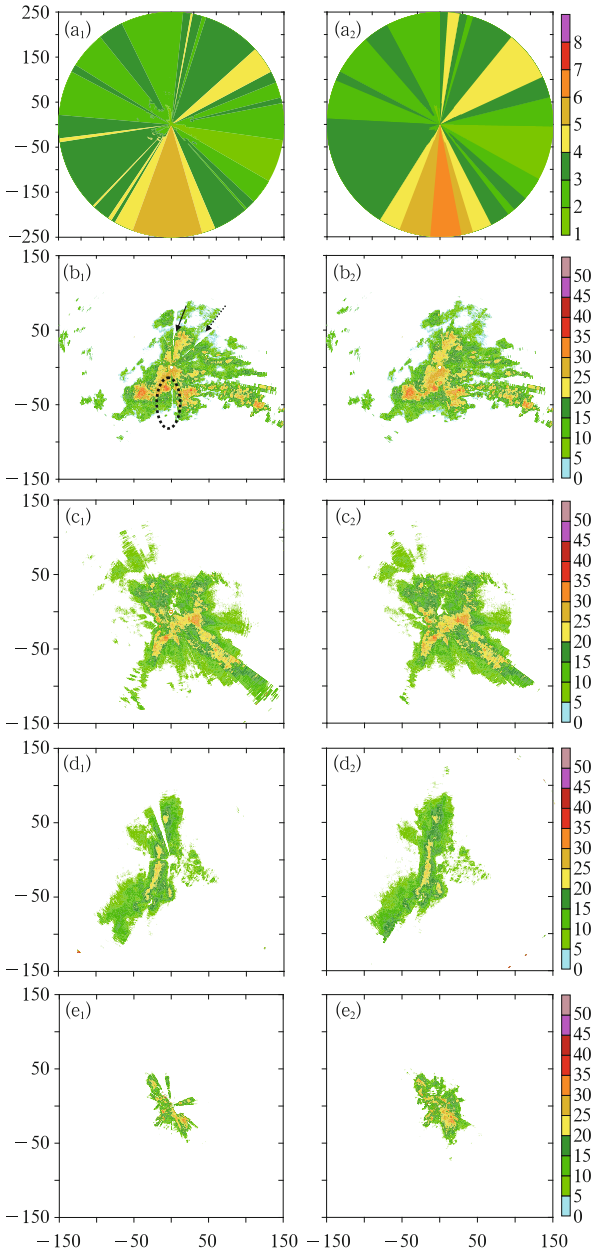

Fig. 5. Hybrid scan elevations according to (a_1) the terrain-based algorithm and (a_2) the reflectivity climatology-based algorithm; terrain-based hybrid scan reflectivity observed by the (b_1) Xining, (c_1) Haibei, (d_1) Naqu, and (e_1) Linzhi radars; reflectivity climatology-based hybrid scan reflectivity observed by the (b_2) Xining, (c_2) Haibei, (d_2) Naqu, and (e_2) Linzhi radars.

tification of hybrid scan elevations that are lower or higher than the actual lowest unblocked elevation by the terrain-based method can lead to V-shaped gaps in HSR or discontinuous reflectivity. Areas experiencing precipitation may be mistakenly judged to be precipitation-free. The results are similar in analyses of HSR observed by the radars at Haibei, Naqu, and Linzhi.

4.2 Statistic analysis method

A statistical averaging method is now developed to further evaluate the effectiveness of the different hybrid scan algorithms. This method is based on the fact that the frequency of precipitation echoes at different unblocked azimuths on the same elevation and at a same range from the radar should not differ greatly. Furthermore, the average reflectivity of different azimuths at the same distance remains roughly constant over sufficiently long periods of time. By contrast, the average reflectivity of azimuths that are partially or completely blocked at the same elevation and range is typically lower than the average reflectivity of unblocked azimuths.

The statistical averaging is performed by accumulating the reflectivity at a given elevation over time, then divided by the number of radar scans included, according to the following formula:

$$\bar{z}(j,i,k) = \frac{1}{n}\sum_{l=1}^{n} z_l(j,i,k), \tag{8}$$

where $z_l(j,i,k)$ is the reflectivity observed in the jth radar bin along the ith azimuth on the kth elevation during the lth of n volume scans, and $\bar{z}(j,i,k)$ is the average reflectivity over those n volume scans. When the value of k is 1, $\bar{z}(j,i,1)$ is the average reflectivity on the first elevation. The index k can be replaced by the terrain-based hybrid scan elevation $k_d(j,i)$, in which case $\bar{z}(j,i,k_d(i,j))$ is the average of terrain-based HSR. Likewise, k can be replaced by the reflectivity climatology-based hybrid scan elevation $k_c(j,i)$, in which case $\bar{z}(j,i,k_c(j,i))$ is the average of the corresponding reflectivity climatology-based HSR.

The average reflectivity of the Xining radar at different elevations and the averages of HSR using both hybrid scan algorithms are calculated from 2034 radar volume scans taken during the 13 large-scale stratiform precipitation events observed at Xining between 2008 and 2010. The results show that the average reflectivity $\bar{z}(80,i,5)$ along the fifth tilt at a location 20

km from the radar (for which the length of the range bin is 0.25 km) changes with the variation of the azimuth (Fig. 6a), as does the average reflectivity at the same range in the sixth tilt ($\bar{z}(80, i, 6)$; Fig. 6b). The terrain-based ($\bar{z}(80, i, k_d(80, i))$; Fig. 6c) and reflectivity climatology-based ($\bar{z}$; Fig. 6d) average HSR values also change with the variation of azimuth.

The frequency of occurrence of reflectivity (FOR; Fig. $1f_1$) and the reflectivity (Fig. $1f_2$) at the sixth tilt indicate that the radar beam on this elevation is not blocked; however, the average reflectivity at this elevation changes with the variation of the azimuth (Fig. 6b), with a range of 20 to 30 dBZ. The variations on the fifth tilt are much larger, consistent with the indication from the FOR and reflectivity at this level that the radar beam is partially blocked near 180°. The average reflectivity near the 180° azimuth drops sharply to less than 10 dBZ (Fig. 6a). This observed reflectivity is substantially weaker than the average reflectivity at the unblocked azimuths on the same tilt, and the difference in reflectivity with azimuth is much larger on the fifth tilt than on the sixth.

These results can be used to analyze the effectiveness and reliability of the two hybrid scan algorithms. The variation of the terrain-based average HSR with azimuth (Fig. 6c) indicates sharp drops to lower than 10 dBZ near the 5°, 45°, and 180° azimuths, suggesting that the radar beams are either completely or partially blocked at these azimuths. This result is consistent with the three V-shaped gaps in the Xining radar observations of terrain-based HSR (Fig. $5b_1$). The climatology-based average HSR also varies with azimuth, but within the range of 20 to 30 dBZ (Fig. 6d). This result indicates that the climatology-based hybrid scan radar beams are unblocked, and is consistent with the continuous spatial coverage provided by the climatology-based HSR observed by the Xining radar (Fig. $5b_2$).

Overall, the application of the reflectivity climatology algorithm provides more accurate calculations of the lowest unblocked elevation and maximizes the utility of radar data within the spatial coverage of the

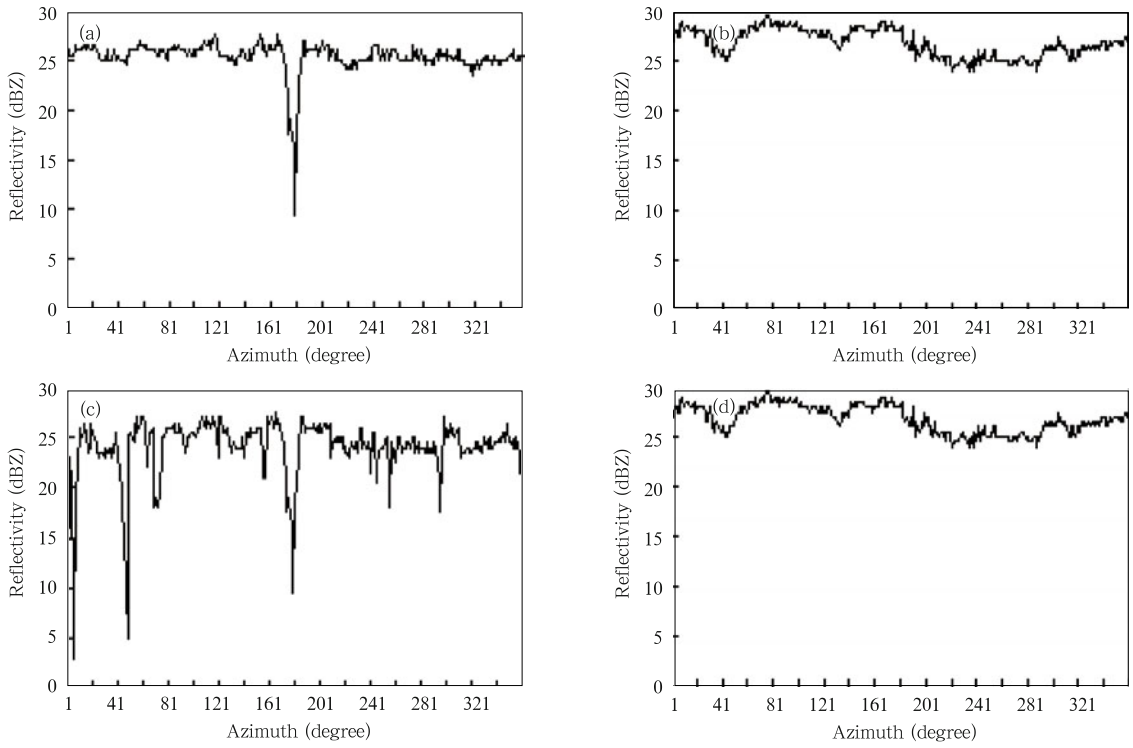

Fig. 6. The dependence of average reflectivity on azimuth according to (a) the fifth tilt, (b) the sixth tilt, (c) the terrain-based HSR, and (d) the climatology-based HSR at a distance of 20 km from the radar site.

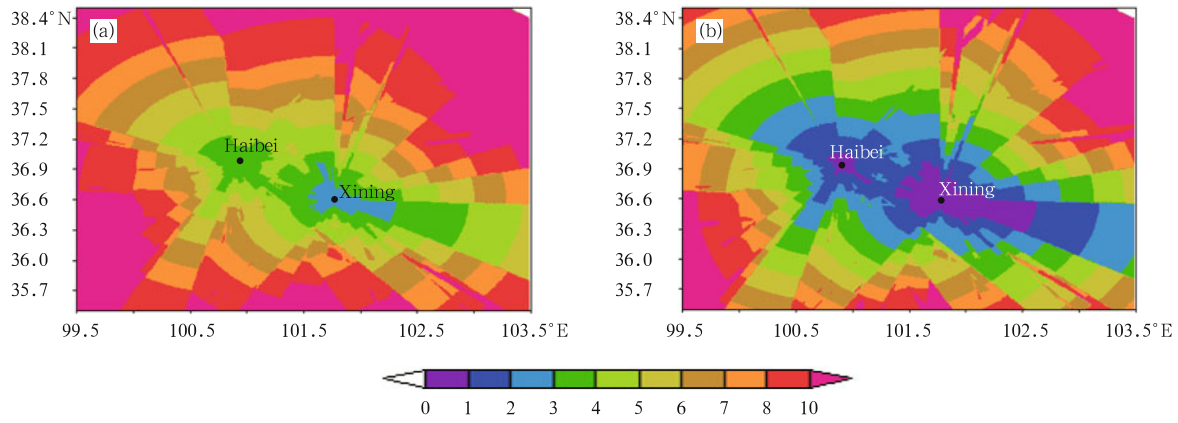

Fig. 7. Mosaic hybrid scan beam heights ($\times 10^3$ m) relative to (a) sea level and (b) the altitude of the Xining radar station over Qinghai.

radar. The hybrid scan reflectivity calculated according to the reflectivity climatology algorithm can be used for radar-based quantitative precipitation estimation (QPE), diminishing the impact of terrain blockage and improving the accuracy of QPE.

5. Doppler weather radar coverage over the Tibetan Plateau

Given appropriate hybrid scan elevations, the beam height H can be calculated with the radar beam height formula under the condition of standard atmospheric propagation. The formula is as follows:

$$H = h + r\sin(\text{elv}) + r^2\cos^2(\text{elv})/(2R_\text{e}), \qquad (9)$$

where h is the altitude of the radar station, r is the slant range, R_e is the equivalent earth radius, and elv is the hybrid elevation angle.

The hybrid scan beam heights from the two Doppler weather radars (Xining and Haibei) are mosaicked to assess radar coverage over the Tibetan Plateau, including Qinghai Province. Observations from the radar with the lower hybrid scan beam height are adopted in cases of coverage overlap. Figure 7a shows the mosaic hybrid scan beam heights above sea level over Qinghai. Most of the radar coverage areas are more than 4000 m above sea level. The altitude of the Xining radar station (2445 m) is lower than that of the Haibei radar station (3123 m); the mosaic hybrid scan beam heights are therefore also reported relative to the altitude of the Xining radar station (Fig. 7b). Figure 7b shows that the areas to the south and northeast of the Xining radar station and to the west of the Haibei radar station have particularly high beam heights. The hybrid scan beam heights of many areas exceed 8 km, where precipitation echoes cannot be detected. The non-uniform distribution of reflectivity vertical profiles is an influential error in radar QPE; thus, the coverage of the Doppler weather radar network in Qinghai is extremely limited. Additional radar or observation data are needed to fill gaps in these regions and minimize the impact of topography to radar QPE.

6. Conclusions

Three months of radar reflectivity data from radars in an area of complex terrain (the Tibetan Plateau) from May to July 2010 were used to develop a reflectivity climatology. This climatology was then applied to the construction of a new hybrid scan algorithm, with the aim of minimizing the impacts of beam blockages. The new hybrid scans were then used to examine the spatial coverage provided by the operational Doppler weather radar network over the Tibetan Plateau. The performance of the reflectivity climatology-based hybrid scans was evaluated relative to the performance of traditional terrain-based hybrid scans. The conclusions can be summarized as follows.

(1) The use of reflectivity climatology in the development of the new hybrid scan algorithm reduced the impacts of beam blockages. Hybrid scans require

the accurate identification of radar coverage. A flexible algorithm based on fuzzy logic concepts was used to discriminate between areas of partial blockage and areas of no blockage. This new hybrid scan method is based on a large volume and long period of radar data, and is independent of both the radar mode and the scan mode. Hybrid scan reflectivity during a large-scale precipitation event was used to validate the new hybrid scan algorithm. The results show that the reflectivity climatology-based algorithm is both effective and reliable, and can be applied to other radars.

(2) Comparison of the reflectivity climatology-based hybrid scan algorithm with the traditional terrain-based algorithm suggests that misidentification of the actual lowest unblocked elevation by the terrain-based algorithm can lead to the V-shaped gaps in the hybrid scan reflectivity. In such cases, areas with active precipitation are mistakenly judged to have no precipitation. The reflectivity climatology-based algorithm provides a more accurate characterization of the lowest unblocked elevation. Further examination of both sets of hybrid scans using a statistical averaging method yielded the same conclusions as the case study. The time-mean terrain-based HSR is substantially lower at some azimuths than at other nearby azimuths. These sharp drops in average HSR are caused by beam blockages. By contrast, the time-mean climatology-based HSR varies much less with azimuth because all azimuths are unblocked. The climatology-based hybrid scan method provides a more accurate measure of reflectivity and enhances the utility of radar data within the radar coverage area.

(3) The coverage of the current weather radar network in Qinghai is extremely limited, as the mosaic hybrid scan heights are high above the ground in most areas. The non-uniformity of vertical reflectivity profiles has long been recognized as a major source of error in radar QPE. Additional radar or other observational data are needed to fill in the gaps in this region, so as to minimize the impact of topography on radar QPE.

Acknowledgments. The authors wish to thank Ms. Liu Hua for translation assistance.

REFERENCES

Bandalo, S., 1992: *An Analytic Method for Radar Horizon Computation: International Weather Radar Networking*. Kluwer Academic Publishers, 75–79.

Chang, P. L., P. F. Lin, B. J. D. Jou, et al., 2009: An application of reflectivity climatology in constructing radar hybrid scans over complex terrain. *J. Atmos. Oceanic Technol.*, **26**(7), 1315–1327.

Fulton, R. A., J. P. Breidenbach, D. J. Seo, et al., 1998: The WSR-88D rainfall algorithm. *Wea. Forecasting*, **13**, 377–395.

Heinselman, P. L., and D. M. Schultz, 2006: Intraseasonal variability of summer storms over central Arizona during 1997 and 1999. *Wea. Forecasting*, **21**, 559–578.

Joss, J., and A. Waldvogel, 1990: Precipitation measurement and hydrology. Radar in Meteorology: Battan Memorial and 40th Anniversary Radar Meteorology Conference, Arizona, Amer. Meteor. Soc., 577–606.

Krajewski, W. F., and B. Vignal, 2001: Evaluation of anomalous propagation echo detection in WSR-88D data: A large sample case study. *J. Atmos. Oceanic Technol.*, **18**, 807–814.

Kuo, J. T., and H. D. Orville, 1973: A radar climatology of summertime convective clouds in the Black Hills. *J. Appl. Meteor.*, **12**, 359–368.

Liu Liping, Feng Jinming, and Chu Rongzhong, 2002: The diurnal variation of precipitation in monsoon season over the Tibetan Plateau. *Adv. Atmos. Sci.*, **19**(2), 365–378.

Maddox, R. A., J. Zhang, J. J. Gourley, et al., 2002: Weather radar coverage over contiguous United States. *Wea. Forecasting*, **17**, 927–934.

Mendel, J. M., 1995: Fuzzy logic systems for engineering: A tutorial. *Proc. IEEE*, **83**, 345–377.

Morin, E., and M. Gabella, 2007: Radar-based quantitative precipitation estimation over Mediterranean and dry climate regimes. *J. Geophys. Res.*, **112**, 1–13.

O'Bannon, T., 1997: Using a "terrain-based" hybrid scan to improve WSR-88D precipitation estimates. Preprints, 28th Int. Conf. on Radar Meteorology, Austin, TX, Amer. Meteor. Soc., 506–507.

Pellarin, T., G. Delrieu, G. M. Saulnier, et al., 2002: Hydrologic visibility of weather radar systems operating in mountainous regions case study for the Ardèche Catchment (France). *J. Hydrometeor.*, **31**(5), 539–555.

Sauvageot, H., 1994: Rainfall measurement by radar. *Atmos. Res.*, **35**, 27–54.

Steenburgh, W. J., S. F. Halvorson, and D. J. Onton, 2000: Climatology of lake-effect snowstorms of the Great Salt Lake. *Mon. Wea. Rev.*, **128**, 709–727.

Xiao Yanjiao, Liu Liping, and Yang Hongping, 2008a: Technique for generating hybrid reflectivity field based on 3-D mosaicked reflectivity of weather radar network. *Acta Meteor. Sinica*, **66**(3), 470–473. (in Chinese)

——, ——, and Shi Yan, 2008b: Study of methods for three-dimensional multiple-radar reflectivity mosaics. *Acta Meteor. Sinica*, **22**(3), 351–361.

Xu Xiangde and Chen Lianshou, 2006: Advances of the study on Tibetan Plateau experiment of atmospheric sciences. *J. Appl. Meteor. Sci.*, **17**(6), 756–772. (in Chinese)

Yang Hongping, Zhang Peiyuan, and Cheng Minghu, 2009: The valid mosaic data region of the CINRAD network. *J. Appl. Meteor. Sci.*, **20**(1), 47–55. (in Chinese)

Zadeh, L. A., 1965: Fuzzy set. *Inf. Control*, **8**(3), 338–353.